Research Article

Investigation of lithological control of iron enrichment in groundwater using geophysical techniques in Yenagoa, Southern Nigeria

K. S. Okiongbo[1] · K. K. Oboshenure[1] · A. R. C. Amakiri[2]

Received: 29 May 2019 / Accepted: 9 December 2019 / Published online: 18 December 2019
© Springer Nature Switzerland AG 2019

Abstract
Hydrochemical analysis of water samples from Yenagoa in the Niger Delta shows widespread occurrence of iron (Fe) in the groundwater. The Fe concentration is more than 0.3 mg/L at many places, and the distribution is heterogeneous both vertically and horizontally. In order to identify the cause of the high heterogeneity, we carried out an integrated study consisting of hydrogeochemical, electrical resistivity sounding and induced polarization (IP) chargeability measurements at eleven sites and 2-D electrical resistivity profiling (at 2 sites). Data processing using inversion techniques resulted in 4-layered resistivity and chargeability—depth models. The results show that clean sand and gravel exhibit high resistivity but low chargeability and normalized chargeability values, whereas clay and sandy clay exhibit relatively low resistivity but high chargeability and normalized chargeability values. In sites where the aquifer is overlain by a thick clay layer, Fe concentration is high (Fe > 0.3 mg/L) in the groundwater and redox potential values range between 118 and 133 mV. We interpret that the low-permeability clay layer creates a relatively atmosphere-isolated state in the underlying aquifer, which is responsible for the reductive ambient subsurface groundwater environment. In sites where the aquifer is capped by silt, Fe concentration is low (< 0.3 mg/L) in the groundwater and redox potential values range between 115 and 164 mv indicating a mild oxidation environment. We interpret that the clay acts as a controlling factor to the Fe enrichment in the groundwater regime. Knowledge of the clay layer, which is identified in the present study, will be helpful in selecting suitable sites for boreholes.

Keywords Groundwater · Electrical resistivity · Induced polarization · Normalized chargeability · Yenagoa

1 Introduction

In the last decade, several investigations were carried out in parts of the Niger Delta, Southern Nigeria, to determine the regulating processes and spatial distribution of Fe in the shallow alluvial aquifer [1, 2]. The results of these studies show that the concentration of Fe in the groundwater abstracted from boreholes is high. Aside, the distribution of Fe in the groundwater was reported to be extremely heterogeneous, both vertically and laterally, within a scale of tens of metres. The issue of high iron concentration (> 0.3 mg/L) in groundwater is a common problem, since over 90% of residents in most cities in the Niger Delta depend on water abstracted from shallow private boreholes. Presently, we remain remarkably ignorant of the cause of the high Fe heterogeneity in the groundwater.

Considering the above, it was pertinent to investigate the probable reasons responsible for the high spatial variation of Fe in the groundwater and provide a sustainable solution for mitigation. Most studies in this direction only concentrated on the geochemical aspects of Fe contamination and suggested various purification techniques for iron removal [3]. Designing various purification methods for iron removal is only temporary solution and suffers

✉ K. S. Okiongbo, okenlani@yahoo.com | [1]Geophysics Research Group, Department of Physics, Niger Delta University, Wilberforce Island, Bayelsa State, Nigeria. [2]Department of Physics, Rivers State University, Port-Harcourt, Rivers State, Nigeria.

from many obvious problems such as waste disposal and maintenance and hence is not a sustainable solution. The strategic importance of groundwater in Yenagoa and the threats posed by excessive Fe concentration emphasize the significance of low-Fe groundwater sources and prompted the assessment of the hydrostratigraphy of the sedimentary sequences in the study area. In assessing the hydrostratigraphy of the sedimentary sequence, it was considered that investigating the alluvial aquifer over short distances ranging between tens to hundreds of metres and in different locations within the study area would perhaps help explain whether the variation in the groundwater Fe concentration was due to local variations in aquifer stratigraphy. Although borehole drilling could be one of the best ways to determine the lithological variation, this approach was considered tedious and would require drilling several boreholes of different depths. This will be time-consuming, laborious and cost-intensive. The use of non-invasive surface geophysical techniques is of great relevance in that reasonably factual subsurface information is obtained without any destruction to the environment within a relatively short time. Electrical resistivity and time domain induced polarization have shown a good complementarity in this regard. The geoelectrical method provides a wide range of variations in the subsurface electrical resistivity. The variations are often associated with water content and lithology; hence, it is one of the most powerful geophysical methods often used in providing solutions to hydrogeological problems [4–6]. Recently, induced polarization method which is based on the chargeability effect of the subsurface has proved to be of significant value in the investigation of lithological variability of unconsolidated sediments especially in the mapping of clay content. In this study, we explore the lithological control on Fe contamination using surface geophysical methods in Yenagoa and environs.

2 Description of the study area

2.1 Location, physiography and climate

Yenagoa is located within the Southern Nigeria sedimentary basin. It is the capital of Bayelsa State. The study area covers an area of about 50 km^2 of Yenagoa, and its metropolis. Yenagoa is bounded by longitudes 006° 10′ 3.07″ and 00 6° 25′ 10.53″ East of the prime meridian and latitudes 04° 51′ 39.73″ and 05°.2′ 25.53″ North of the equator. Geographically, Yenagoa is within the coastal area of the Recent Niger Delta (Fig. 1) where the ground surface is relatively flat, sloping very gently seawards [7]. Its mean elevation is about 8 m above the mean sea level [8]. The study area has a tropical rain forest climate characterized by rainy season and dry season. The rainy season commences from April to October with a brief dry period in August. The dry season lasts between November and March. The mean annual rainfall is about 4500 mm [9] and about 85% of the mean annual rain falls during the wet season. The temperature varies between 25 and 32 °C. Fishing and farming are the main occupation of the people.

2.2 Geology and hydrogeology of the study area

The study area lies within the fresh water swamps, backswamps, deltaic plain, alluvium and meander belt geomorphic unit of the Niger Delta [9]). The Niger Delta is basically an alluvial plain and consists of the modern and Holocene delta top deposits. Grain-size profiles of the Holocene alluvial deposits consist of a fining-up sequence of sand capped by fine silts and clay indicating a fluvial environment of deposition [10]. The fine-grained silts and clay overlying the basal sandy sequence are often called the near surface aquitard. The near surface aquitard thickness varies between < 5 to about 12 m, and due to the varying clay, silt and fine sand content, [10] reported that the aquitard permeability is highly heterogeneous. The near surface aquitard becomes a confining unit if it is thick and impermeable, which prevents percolation of precipitation into the alluvial aquifer. Akpokodje [9] reported that groundwater flows from North to South in the region.

Three main subsurface lithostratigraphic units are reported in the Niger Delta [11]. From top to bottom, they are Benin, Agbada and Akata Formations. The Benin Formation which is fluvial in origin is the main aquifer. Groundwater occurs mainly under unconfined conditions in the Benin Formation. Abam [12] observed that the sediments of the Benin Formation were deposited during the Late Tertiary–Early Quaternary period and are about 2100 m thick. The sediments are lenticular and unconsolidated and consist of coarse- to medium-fine-grained sands with localized intercalations of clay/shale. Gravel and pebbles are minor components. Mbonu et al. [13] reported that the sands are moderately sorted and poorly cemented. The presence of thin clay beds creates discontinuities in the vertical and lateral continuity of the aquifer, resulting in the presence of local perched aquifers [10]. The aquifer is directly recharged through the infiltration of rain water. In the Niger Delta, the water table in many areas is close to the surface though subject to seasonal variations. The water table is about 3–4 m in the dry season [14], but rises considerably in the rainy season. Groundwater is the main source of drinking water for over 80% of the population in the study area.

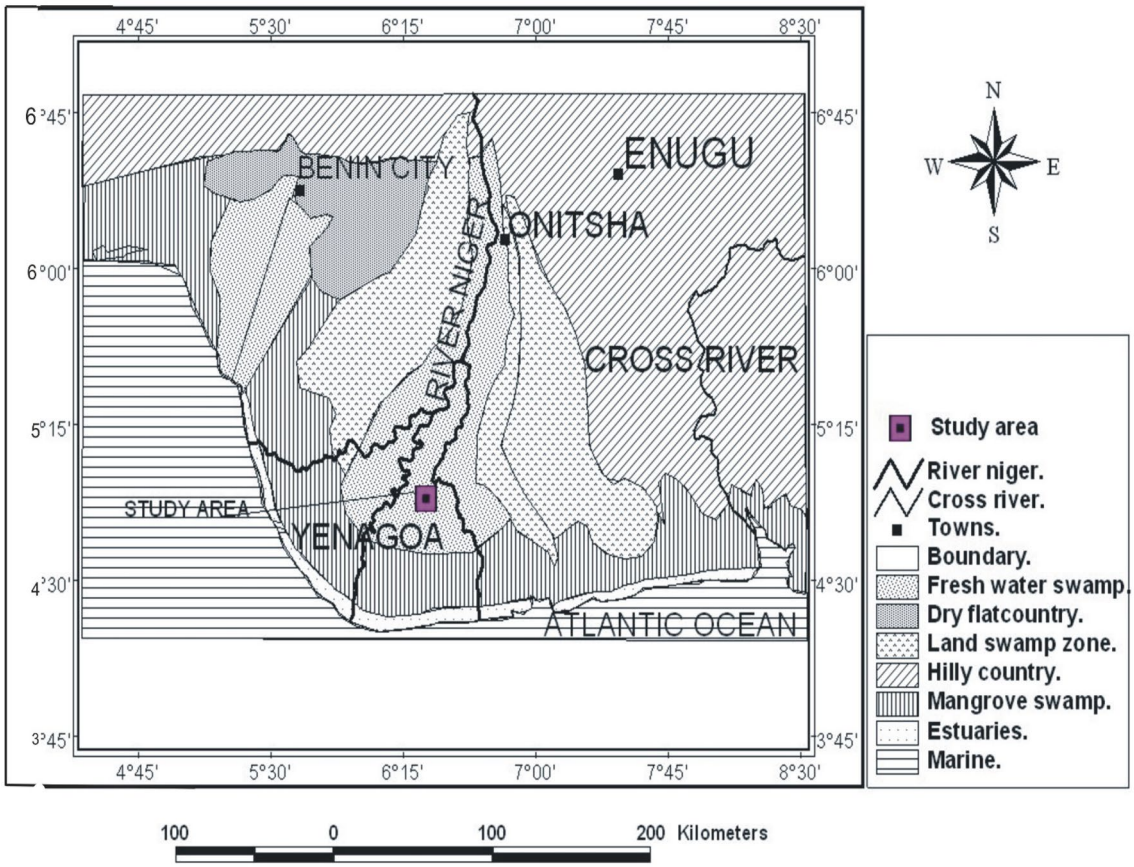

Fig. 1 Map of the Niger Delta showing the study area

3 Induced polarization (IP) method

In the electrical method of geophysical prospecting, current is injected using two current electrodes A and B. The passage of the electric current through the ground creates a potential difference (ΔV) usually measured across a pair of potential electrodes C and D. If the inducing current is turned off, the difference of potential (ΔV) does not immediately drop to zero, but decays slowly over a period of time. The recording of the decaying voltage gives a decay curve $\Delta V_{ip}(t)$. In time domain surveys, the decay curve $\Delta V_{ip}(t)$ is the object of study because it is characteristic of the medium in terms of initial magnitude, slope and relaxation time. The amplitude of ΔV_{ip} is related to the polarizability of the earth materials [15]. This capacity to polarize is referred to as the IP response. The form of the primary wave and the IP decay is shown in Fig. 2. Induced polarization is due to two main sources: (1) membrane polarization and (2) electrode polarization. The presence of clay causes membrane polarization. The clay particles, which are negatively charged, attract positive ions from the electrolytes in the capillaries of the clay particles and thus behave as ion-selective membrane impeding their mobility through the capillaries.

Electrode polarization produces similar effect but occurs when metallic minerals are present. The flow of electrons through a metal is much faster than the flow of ions in the electrolyte, and hence, opposite charges accumulate on the surface of metallic grains that block the path of ionic flow through the pore fluid. In Fig. 2, the chargeability M is computed by integrating the signal V_{ip} along the decay over n time windows, or gates. The chargeability of IP effect was measured by integrating the area under the IP decay curve according to the relation [16, 17] given below:

$$M = \frac{1}{V_o}\int_{t1}^{t_2} V(t)\mathrm{d}t \tag{1}$$

where V_o is the voltage measured before the current is turned off, t_1 and t_2 are the start and stop time intervals, respectively, and $V(t)$ is the decaying voltage. The chargeability (M) is usually expressed in millisecond (msec) or milliVolt/Volt (mV/V).

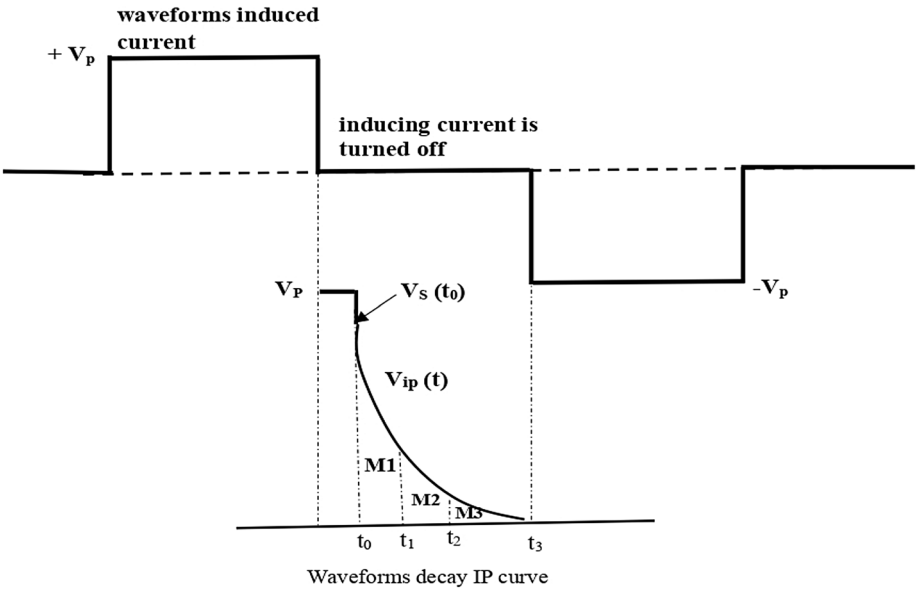

Fig. 2 Time domain IP discharge curve

4 Data acquisition and processing

Prior to the acquisition of geophysical data and drilling of boreholes, locations with contrasting dissolved Fe concentration (low and high) in the groundwater within Yenagoa and environs were selected for study. The selection of these locations was based on analysis of ten groundwater samples collected from the existing domestic boreholes spread over the study area. The depths of these boreholes range from 9 to 30 m. Geochemical analysis of the groundwater samples shows that groundwater from Tombia, Akenfa III, etc., (Fig. 3) exhibits Fe concentration within WHO acceptable limits (~ 0.02–0.3 mg/L), while groundwater samples from Amabolou, Azikoro, etc. (Fig. 3), have Fe concentrations greater than 0.3 mg/L. This analysis helped in planning the field layout of the geophysical profiles.

4.1 Geoelectrical sounding and induced polarization

We acquired geoelectrical and IP data in eleven locations, i.e. five in low-Fe areas and six in high-Fe areas (Fig. 3). The electrical resistivity–IP soundings were carried out using the Schlumberger configuration. In general, soundings were carried out using the Abem Terrameter SAS 1000. Maximum current electrode separation AB/2 ranged between 100 and 150 m. In the Schlumberger configuration, current was injected into the ground through two outer electrodes A and B and the resulting voltage difference at two potential electrodes (C and D) was measured. An increase in the depth of current penetration is achieved by progressively increasing the electrode spacing. Field precautions observed to ensure good vertical electrical sounding (VES) data quality included firm grounding of the electrodes and checking for current leakage and creeps to avoid spurious measurements. During the survey, the resistance and chargeability were measured concurrently. These data were interpreted using IX1D (Interpex) software. The field resistivity data were converted to apparent resistivity (ρ_a) values and plotted against half-current spacing (AB/2) on log–log scale. Guided by the general trend of the field curves, partial curve smoothening of the field curves was made. The 1D inversion software (Interpex) takes advantage of least-squares optimization technique. The program iteratively compares the field data to a theoretical model curve. The starting model is modified or adjusted successively until the difference between the observation and the model output is reduced to a minimum. In constructing a model, we have used the principle that all maxima, minima and point of inflexion in a geoelectrical sounding curve indicate the existence of boundaries of different lithologies. Using this approach, the subsurface was divided into a number of horizontal layers of given thickness. The program iteratively changes the resistivities to obtain a best fit with the field data for the layer thicknesses chosen for the model. Due to the inherent problem of equivalence in geosounding data interpretation [18], lithological information from drilled boreholes was used to constrain all depth estimates in order to minimize the choice of equivalent models by fixing layer thicknesses and depths while allowing the resistivities to vary [19]. The resulting true resistivities represent

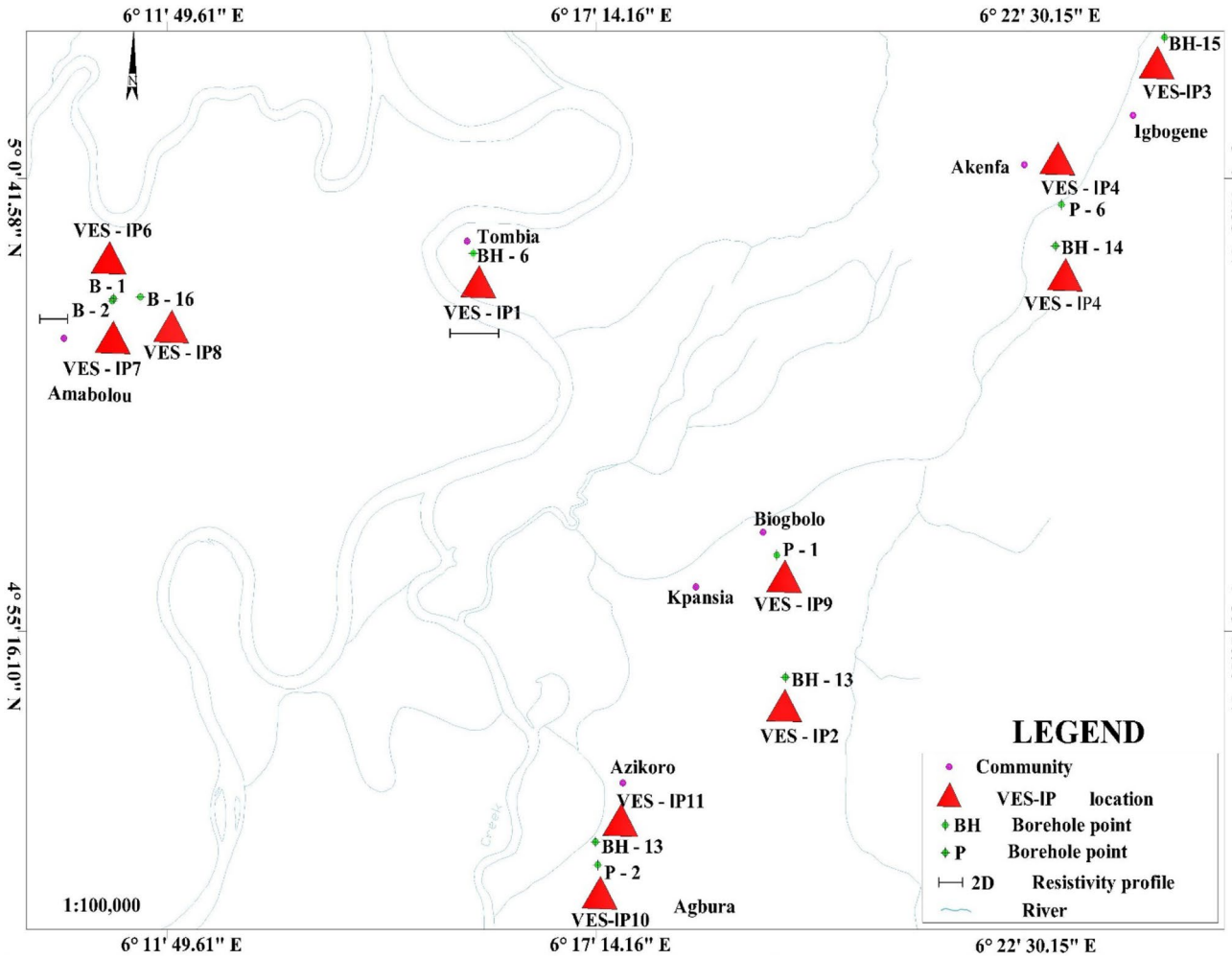

Fig. 3 Map of study area showing VES-IP sounding, borehole locations and 2D traverses

Table 1 Summary of VES-IP model results and their corresponding thicknesses at low-Fe areas

VES-IP No	Layer 1 (top soil)				Layer 2 (silty sand)				Layer 3 (sand)				Layer 4 (sandy clay)				
	ρ (Ωm)	η (ms)	*MN* (mS/m)	*h* (m)	ρ (Ωm)	η (ms)	*MN* (mS/m)	*h* (m)	ρ (Ωm)	η (ms)	*MN* (mS/m)	*h* (m)	ρ (Ωm)	η (ms)	*MN* (mS/m)	*h* (m)	RMS error (%)
VES-IP 1	33	0.79	0.024	0.5	295	3.8	0.013	0.8	2955	4.2	0.001	8.0	50	10.8	0.216	–	5.8600
VES-IP 2	34	2.43	0.071	0.9	167	1.84	0.011	1.3	415	1.24	0.003	17.6	138	45.36	0.329	–	5.2182
VES-IP 3	19	0.26	0.014	0.7	19	3.54	0.186	2.1	352	11.25	0.031	6.1	298	126.3	0.424	–	4.3275
VES-IP 4	43	2.47	0.057	0.7	141	1.30	0.009	1.6	268	0.71	0.003	13.2	85	10.1	0.119	–	4.6978
VES-IP 5	29	1.82	0.063	1.1	28	1.82	0.065	6.6	219	1.75	0.008	27.0	253	1.72	0.007	–	2.8988

ρ is bulk resistivity, η is chargeability, *MN* is normalized chargeability, and *h* is thickness

the best average resistivity for the given layer and are shown in Tables 1 and 3, respectively.

Because the chargeability represents a measure of polarization magnitude relative to conduction magnitude [17, 18] and thus is approximately linearly related to the bulk resistivity, we also calculated the normalized chargeability (MN), using the following expression:

$$MN = \frac{M}{\rho}(mS/m) \quad (2)$$

to separate the effects of conduction and polarization. Where M is the chargeability and ρ is the layer bulk resistivity.

4.2 Electrical resistivity imaging

We also acquired one each 2D electrical resistivity imaging profile in the low-Fe area and as well as in the high-Fe area using the Wenner array (Fig. 3). The 2D resistivity profile was acquired to supplement the vertical electrical sounding (VES) and IP sounding data. This is because the 2D resistivity imaging gives a clearer picture of the lateral and vertical variation of the subsurface geological sequences. The 2D resistivity imaging data were acquired manually using the Wenner configuration. Each 2D profile was 100 m in length. The electrode separation ranged between 5 and 30 m in an interval of 5 m, with a total of 21 electrode positions for each profile. Field measurements were taken using electrode spacing of 5.0 m at electrode positions 1, 2, 3 and 4 in each profile. Then, each electrode was moved a distance of 5.0 m (one unit electrode spacing), the active electrode positions being 2, 3, 4 and 5. This procedure was continued to the end of the profile with electrode positions for the last measurement being 18, 19, 20 and 21. The electrode spacing was then increased by 5.0 m, as mentioned above for measurements of next data level, such that the active positions were 1, 3, 5 and 7. The procedure was then repeated by moving each of the electrodes a distance 5.0 m (one unit electrode spacing) and maintaining the electrode spacing for the data level until the electrodes were at electrode positions 15, 17, 19 and 20. This procedure was continued until 6 data levels were observed, yielding a total of 63 data points in each of the profiles. RES2DINV computer code [19] was used in the inversion of the 2D data. The computer program takes advantage of the nonlinear optimization technique in which a 2D resistivity model of the subsurface is automatically determined for input apparent resistivity data [19, 20]. In this program, the subsurface is subdivided into a number of rectangular blocks based on the spread of the observed data. The 2D data were inverted using the least-squares inversion with standard least-squares constraint which minimizes the square difference between the observed and the calculated apparent resistivity values. The program displays the distribution of electrical properties in the form of 2D pseudo-section plot. 2D pseudo-section plot gives a simultaneous display of both horizontal and vertical variation of the subsurface resistivity and are useful for initial quality assessment [21]. In constructing a 2D pseudo-section plot, each measured value is put at the intersection of two 45° lines through centres of the quadripole. Each horizontal line is then associated with a specific value of n (inter electrode spacing) and gives a pseudo-depth of investigation. It is pertinent to note that the larger the *n*-values, the greater the depths of investigation [21].

4.3 Hydrogeochemical analysis

Eleven boreholes were drilled in the study area using rotary drilling method. Five boreholes were drilled in the low-Fe areas, while six were drilled in high-Fe areas. Each borehole was located close to a VES point. The locations of the boreholes in the low-Fe areas are Tombia, Kpansia (behind the market along the expressway), Igbogene, Akenfa III and Akenfa III (NNPC Road), while the high-Fe areas include Amabolou I, II and III, Biogbolo, Agbura and Azikoro (Fig. 3). The boreholes were developed, and groundwater samples were collected in clean 500-ml polyethylene bottles. Prior to sample collection, the boreholes were pumped continuously for about 10–20 minutes. In these samples, in situ measurements of temperature, redox potential (Eh) and pH were taken using precalibrated portable pH/ORP meter at the time of groundwater sampling. Major ions such as Na, K, Ca, Mg, Fe, HCO_3, Cl and SO_4 were determined including total dissolved solids (TDS) in the laboratory using standard procedures [22]. Major ions like sulphate (SO_4^{-2}) were determined by spectrophotometric turbidimetry. Using EDTA, calcium (Ca^{2+}) and magnesium (Mg^{2+}) were determined titrimetrically; chloride (Cl^-) was determined by standard $AgNO_3$ titration and bicarbonate (HCO_3^-) was determined using titration with HCl. Sodium (Na^+) and potassium (K^+) were measured using flame photometry; nitrate (NO_3^-) was determined by colourimetry with a UV–visible spectrophotometer (brucine method) while iron was measured using colourimeter with a UV–visible spectrophotometer at 520 nm. Subsequently, the groundwater composition was correlated with the colour characteristics of the sediments. Chemical composition of the groundwater at the low- and high-Fe areas as well as the redox potential values is shown in Tables 2, 4 and 5, respectively.

The drilled boreholes were lithologically logged and sampled at 3.0 m or more often when characteristics of the sediment changed based on their grain size and colour. Each sample was assigned to one of the three colours—grey, off-white and brown by virtual inspection of the sediments. The Fe concentration of about 3 g of the wet sediments was measured by AAS and after extraction with hydroxylamine hydrochloride ($NH_2OH.HCl$) in 25% acetic acid, and filtering using a 0.45-µm cellulose acetic filter. The boreholes were screened at depth intervals of either oxidized brownish sand aquifers, off-white

Table 2 Chemical composition of the groundwater at low-Fe areas

VES-IP No	Borehole No	Depth (m)	pH	Eh	EC	TDS	TA	Na^+	K^+	Ca^{2+}	Mg^{2+}	Fe	Cl^-	SO_4^{2-}	NO_3^-	HCO_3
VES-IP 1	BH-6	8	6.48	164	197	99	98	5.3	1.7	9.6	3.4	0.16	10	6.54	0.32	1.8
VES-IP 2	BH-13	27	6.04	157	148	74	6	2.7	4.2	7.3	3.1	0.14	19	3.6	0.11	0.5
VES-IP 3	BH-15	24	6.42	148	167	84	10	2.3	6.3	10.2	6.5	0.26	16	4.8	0.18	0.7
VES-IP 4	BH-14	20	6.4	115	274	137	15	5.4	1.3	12.5	2.8	0.2	17	3.2	0.22	1.8
VES-IP 5	P-6	12	6.58	142	32	160	4	9.8	4.6	21.5	5.5	0.22	30	10.7	0.14	0.5

All parameters have been expressed as mg/L except pH, EC and Eh. The unit of EC is µS/cm, and that of Eh is mV

or greyish reduced sediments. The depth of these boreholes varied between 8 and 30 m. Fe concentration in the aquifer sediments is shown in Table 5.

5 Results and discussion

In this study, resistivity soundings and profiling were carried out in locations with contrasting dissolved iron concentrations, low and high in the groundwater (Fig. 3). IP soundings were also carried out simultaneously to support

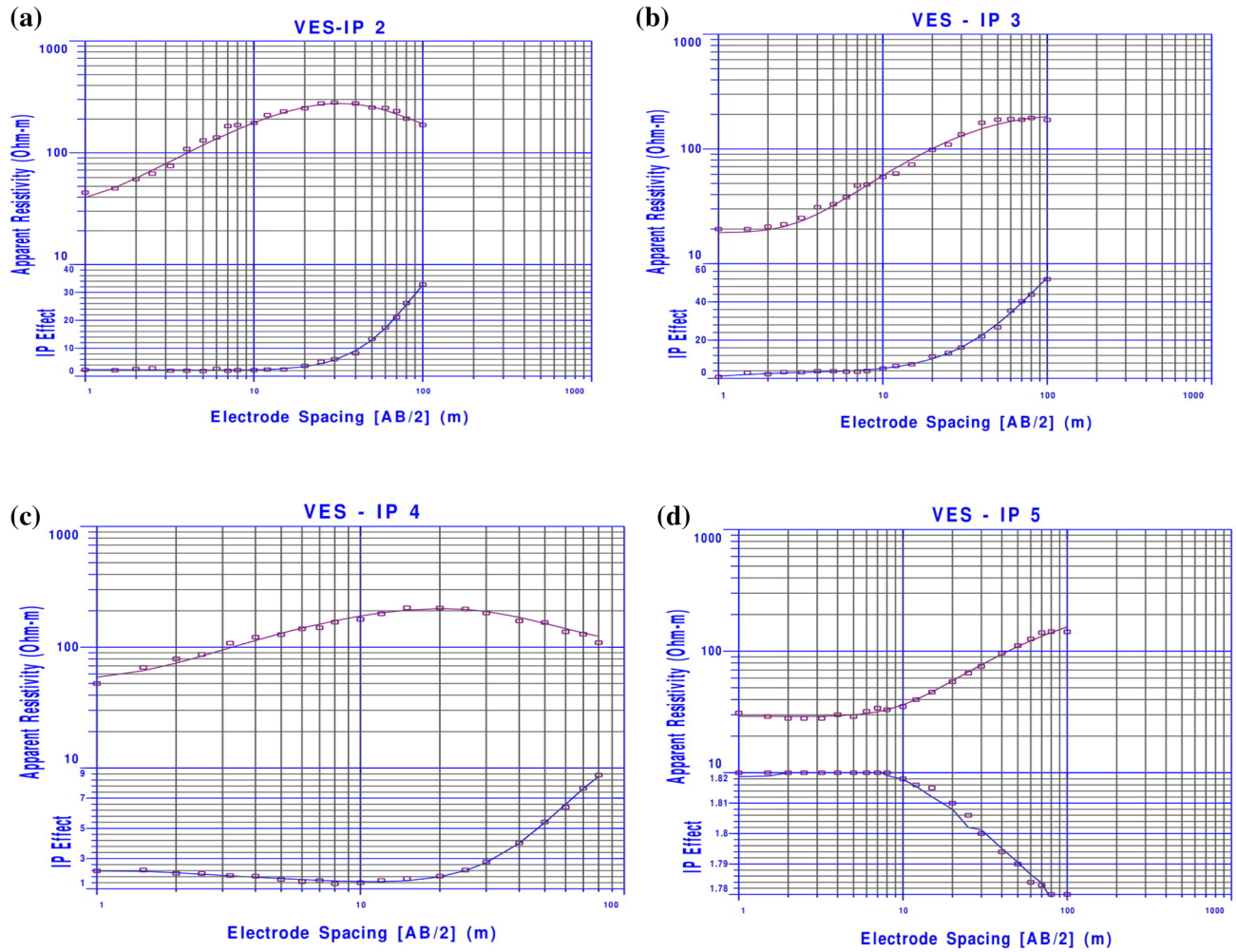

Fig. 4 Resistivity and IP sounding curves in the low-Fe areas

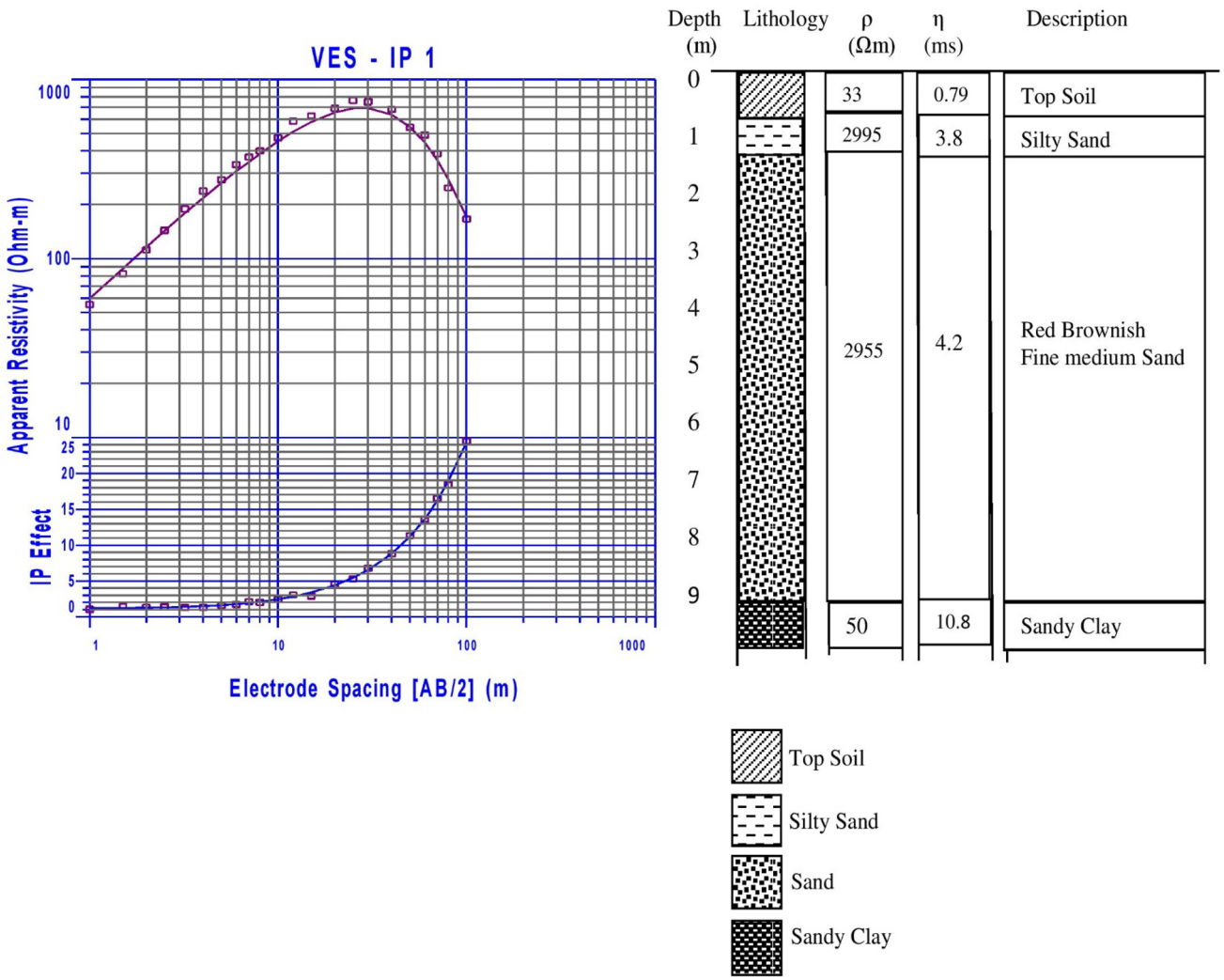

Fig. 5 Resistivity–IP Sounding at Tombia Village (VES-IP 1, low-Fe area); **a** resistivity–IP model curves compared to field data; **b** model VES-IP results with borehole log and lithologic interpretation shown for comparison

the resistivity interpretation for investigating the lithological control of Fe enrichment in the groundwater.

Figure 4 shows resistivity and IP sounding curve types in locations where the dissolved Fe concentration is low, while Fig. 5 shows resistivity/IP curve, and a comparison between the I-D resistivity/IP model of VES-IP 1 (Table 1) with the lithological information obtained from the nearest borehole (B-6) in Tombia (Fig. 3). The I-D inversion results for the Schlumberger resistivity/IP soundings and results of the hydrochemical analysis from groundwater samples from boreholes near the resistivity/IP sounding points in the low-Fe areas are also presented in Tables 1 and 2, respectively. Correlation of the resistivity results of VES-IP1 with the lithological information from the nearest borehole (B-6) shows that the stratigraphic sequence consists of four layers (within the depth of investigation) in which the model resistivity of the third layer is higher than those of the upper and lower layers (Fig. 5). The resistivity curve obtained in this area is predominantly K-type (Fig. 4), and the stratigraphic sequence consists of top soil, silty sand, sand and a sandy clay (Fig. 5). The resistivity and thickness of the top soil vary between 19 and 43 Ωm and 0.5–1.1 m, but are 19–295 Ωm and 0.8–6.6 m in the silty sand layer underlying the top soil (Table 1). The resistivity and thickness of the sandy layer which serves as the aquifer vary between 219 and 2955 Ωm and 6.1–27 m, respectively, while the resistivity of the sandy clay layer ranges between 50 and 298 Ωm. The 2D resistivity cross section (Fig. 6) correlated well with the borehole information (Fig. 5) and shows the detailed variation of the subsurface lithological sequence. Figure 6 shows a clear trend of high apparent resistivity values at the top (values ranging between 200 and 680 Ωm), while at the bottom, the apparent resistivity values tend to decrease (values are lower

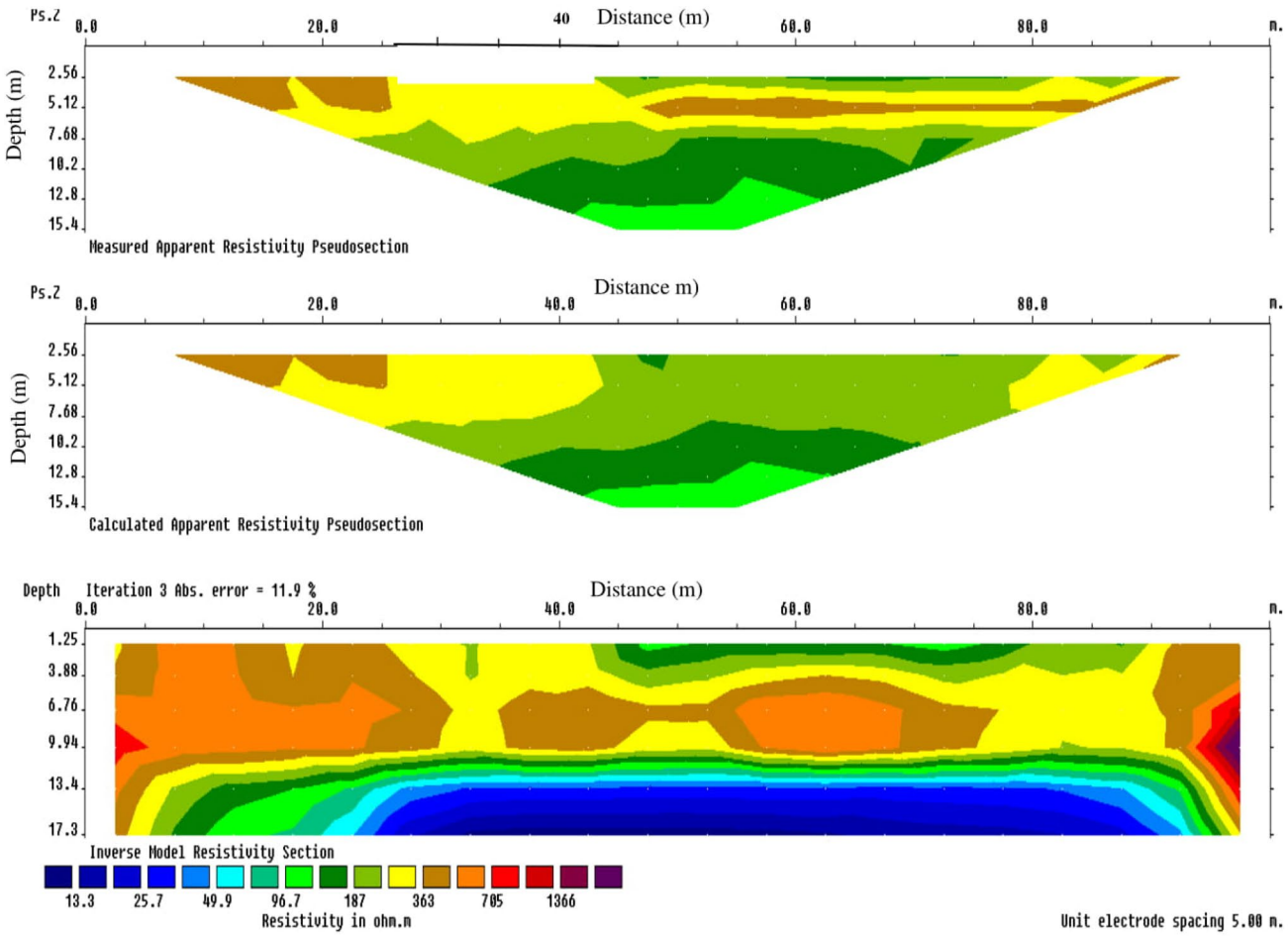

Fig. 6 Inverse model resistivity section at Tombia Village (low-groundwater Fe site). The vertical line indicates the location of borehole

than 100 Ωm). Correlation of the 2D resistivity cross section with the lithological information from the borehole located close to the profile line (Fig. 5) indicates that the top soil with an apparent resistivity range of 80–100 Ωm is underlain by a layer with an apparent resistivity range of 150–200 Ωm. The borehole data indicate that this layer is composed of silty sand. The apparent resistivity of the layer below the silty sand layer varies between 300 and 1000 Ωm. This layer serves as the aquifer and consists of sand. Below the aquifer is a layer with apparent resistivity range less than 100 Ωm. The lithological information from the borehole shows that this layer is a sandy clay layer.

The chargeability (*M*) and normalized chargeability (*MN*) of the top soil range between 0.79 and 2.47 ms and 0.014–0.073 mS/m but range between 1.3 and 3.8 ms and 0.009–0.186 mS/m, respectively, in the silty sand layer. In the sandy layer, the chargeability and normalized chargeability values are between 0.71 and 11.25 ms and 0.001–0.031 mS/m but range between 1.72 and 126.3 ms and 0.007–0.424 mS/m in the sandy clay layer. The chargeability of a given medium indicates polarizability of the medium. Thus, chargeability is related to the permittivity and resistivity of the subsurface materials as well as the porosity and moisture content in the subsurface media. The normalized chargeability (i.e. the ratio between chargeability and resistivity) has also been reported to be a good parameter for discriminating lithotypes [17, 18]. These authors suggested that clean sands have low chargeability and low normalized chargeability, while clay and clayey sands have high chargeability and normalized chargeability values.

A careful analysis of the model results (Figs. 5 and 8) shows a strong correlation between the resistivity and chargeability anomalies with high resistivity values corresponding to relatively low chargeability and normalized chargeability values (Table 1). Deposits of clean sand and gravel are easily distinguished by their high resistivity values from their surrounding clay and silt [23–25]. Small measurable IP effects are associated with clean sand and gravel deposits [26]. The model results show low

chargeability and low normalized chargeability values in the second and third layers (i.e. silty sand and sand layers). This indicates that these layers are mainly composed of sandy materials and less disseminated clayey materials. In contrast, high chargeability and normalized chargeability values are observed in the sandy clay layer ranging between 1.72 and 126.3 ms and 0.007–0.424 mS/m relative to layers 2 and 3. This is consistent with the observation of Amaya et al.; Vonhala [26, 27] who suggested that strong IP effects are commonly observed in sediments containing clays disseminated on the surface of larger grains. Hence, the sandy clay layer displays large IP effects as a result of the presence of disseminated clay. The lithology suggested by the 2D resistivity interpretation (Fig. 6) correlated well with the observed subsurface materials obtained from ground-truthing in this location and also clearly delineate the basal sandy clay layer. Layer 3 serves as the aquifer in the area, and residents tap their water from this layer. Table 2 shows that the Fe concentrations obtained from the analysis of groundwater samples abstracted from boreholes in these areas are within WHO acceptable limits. Additionally, the measured redox potential values from the groundwater immediately after abstraction are relatively high, ranging between 115 and 164 mV, indicating a mild oxidation environment [28].

Figure 7 shows resistivity–IP sounding curves in locations that have high Fe concentration in the groundwater. For comparative study, IP sounding curves are presented along with resistivity sounding curves. Figure 8 shows field data, I-D inversion results for Schlumberger resistivity/IP sounding at Amabolou (VES-IP 6), a high-Fe-concentration area. The resulting I-D resistivity/IP model was compared to the borehole lithological information. Interpretation of the resistivity and IP sounding curves shows a large variation in resistivity and chargeability and hence normalized chargeability. Generally, resistivity, chargeability and normalized chargeability values vary between 5 and 2288 Ωm, 0.7–204 ms and 0.016–2.722 mS/m, respectively (Table 3). In Fig. 7, we observed that for values of AB/2 greater than 5 m, the resistivity and polarization curves have opposite slopes. The top soil is relatively dry and resistive and unpolarizable, but the lower layer, being wet, is lower in resistivity and high in polarizability. The low-resistivity anomaly and enhanced IP and normalized chargeability effect is attributed to the cationic exchange capacity due to the increase in clay volume [26].

Clay and clayey sand display large IP effect due to cationic exchange capacity [26, 27]. Table 3 shows that beside the top layer, the underlying layers, especially layers 2 and 3, have high chargeability and normalized chargeability values reflecting enhanced surface polarization caused by the presence of disseminated clay. Of particular interest with respect to the hydrogeology and the mobilization of Fe in the aquifer is the second layer, characterized by low resistivity (5–96 Ωm) and high chargeability and normalized chargeability values (0.67–13.9 ms and 0.039–2.242 mS/m). The correlation of VES-IP 6 interpretation results with the nearest lithological information (Fig. 8) shows that layer 2 is clay. The significant correlation of low resistivity and high chargeability affirms also that this layer is clay. The 2D resistivity cross section (Fig. 9) shows that underlying the top soil is a layer characterized by low apparent resistivity values in the depth range of about 2.5–7.8 m corroborating the results of the vertical electrical sounding (VES). The apparent resistivity values are generally less than 60 Ωm. The lithological information from the nearest borehole (Fig. 8) shows that this layer is a clay layer. Underlying the clay layer is a layer with slightly higher apparent resistivity values ranging 60–120 Ωm within the depth range of 8–13 m. The borehole data indicate that this layer is composed of fine sand in a matrix of finer sediments (clay) [29]. Below the sandy clay layer is the sandy layer with apparent resistivity range of about 120–220 Ωm. This clay layer (aquitard) acts as a confining layer. Analysis of groundwater samples abstracted from the sandy layer below the clay layer show elevated concentrations of dissolved Fe (Table 4). Redox potential values are relatively low and range between 116 and 133 mV, indicating a mild reducing environment. It is pertinent to mention that in the present study, analysis of the normalized chargeability results (Tables 1 and 3) did not give a clear difference of normalized chargeability values in layers with high clay content and coarse material in some layers contrary to the report of [26]. For instance, in VES-IP 7, 9 and 10 layer 2, results of the normalized chargeability did not show a clear trend of increasing values in this layer with high clay content and lower values when coarse material is the main soil content (VES-IP 9, 10 layer 4) and thus did not contribute significantly to the interpretation of the geological features in these layers. However, normalized chargeability values in these layers were used to complement the results of the chargeability.

5.1 Source of Fe and role of near surface clay layer on groundwater Fe distribution

Fe concentrations were extracted from aquifer sediments from both the low and high locations. The results show that Fe concentrations in the high-Fe aquifer sediments range between 0.26 and 0.90 mg/L but are between 0.5 and 0.82 mg/L in the low-Fe aquifer sediments. Table 5 lists the Fe concentrations in several sediment samples from borehole cores and indicates that aquifer sediments containing abundant Fe act as the supply source for the shallow groundwater. There is no significant overall difference in the amount of extractable Fe in the aquifer sediments.

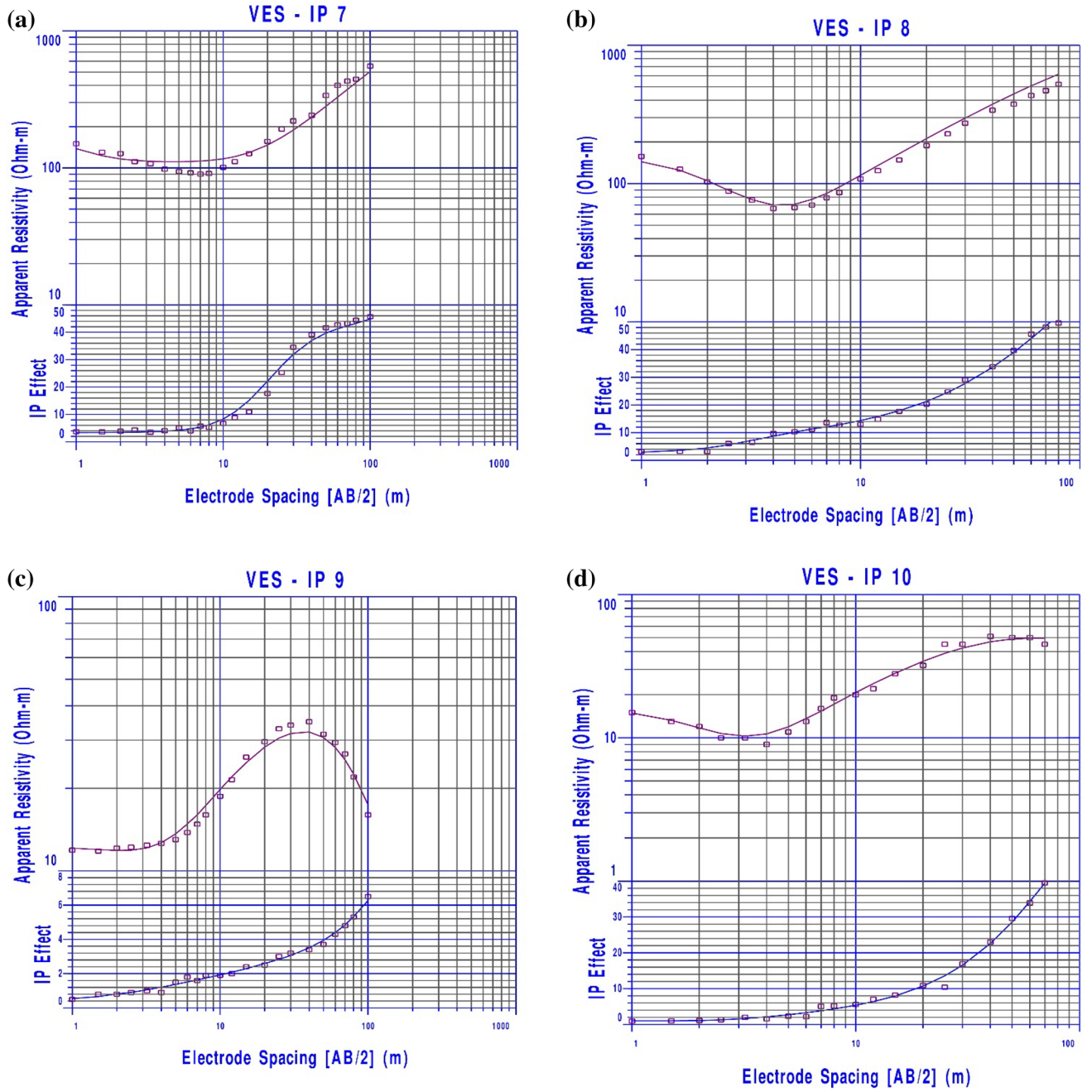

Fig. 7 Resistivity and IP sounding curves in the high-Fe areas

This is consistent with the studies of [27] who reported that paralic deposits often have plenty of Fe substances. The similar amount of extractable Fe in the aquifer sediments implies that Fe is present in the aquifer materials in sufficient amounts. Thus, transfer to the dissolved phase can cause a large increase in groundwater.

We infer therefore that the spatial distribution of groundwater Fe is as a result of the variation of redox conditions in the host aquifer. This implies that a reductive ambient subsurface environment is favourable to Fe ions transferring from the aquifer matrix into the groundwater. Although the decomposition of organic matter in groundwater and soil can consume dissolved oxygen and thus create a reductive hydrochemistry, in this case this effect is assumed to be significantly small. We opine that a relatively atmosphere-isolated state in the aquifer is responsible for the stronger reducibility of groundwater in the high-Fe locations. The investigations of the sediment

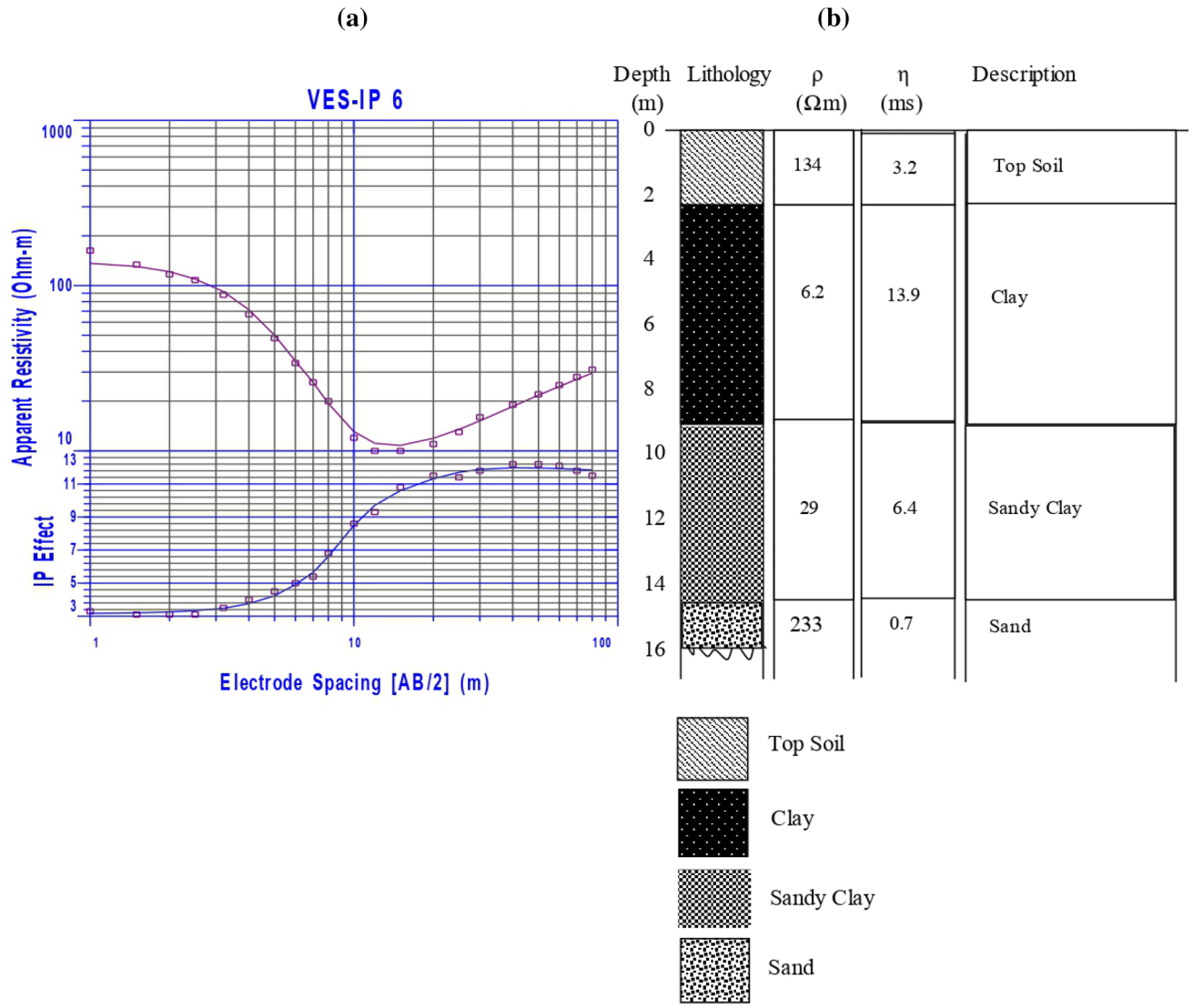

Fig. 8 Resistivity–IP sounding at Amabolou Village (high-Fe area); **a** resistivity–IP model curves compared to field data; **b** model VES-IP results with borehole log and lithologic interpretation shown for comparison

Table 3 Summary of VES-IP model results and their corresponding thicknesses at high-Fe areas

VES-IP no	Layer 1 (top soil)				Layer 2 (clay)				Layer 3 (sandy clay)				Layer 4 (sand)				RMS error(%)
	ρ (Ωm)	*η* (ms)	*MN* (mS/m)	*h* (m)	*ρ* (Ωm)	*η* (ms)	*MN* (mS/m)	*h* (m)	*ρ* (Ωm)	*η* (ms)	*MN* (mS/m)	*h* (m)	*ρ* (Ωm)	*η* (ms)	*MN* (mS/m)	*h* (m)	
VES-IP 6	134	3.20	0.024	2.2	6.2	13.9	2.242	6.6	29	6.4	0.221	5.4	233	0.7	0.021	–	5.0357
VES-IP 7	181	3.80	0.021	0.7	96	3.70	0.039	10.1	643	90.9	0.141	8.9	2288	204.1	0.089	–	4.3482
VES-IP 8	158	2.60	0.016	1.2	46	9.30	0.202	3.7	960	62.5	0.065	9.5	1433	176	0.123	–	3.7921
VES-IP 9	12	0.49	0.041	1.0	11	1.20	0.109	2.8	49	4.2	0.086	27.1	45	8.1	1.400	–	5.7832
VES-IP 10	19	1.05	0.055	0.6	5	0.67	0.134	2.0	122	26.7	0.219	9.3	56	73.9	1.320	–	2.9105
VES-IP 11	52	1.60	0.031	0.7	12	9.70	0.808	1.3	9	24.5	2.722	21.2	226	12.5	0.055	–	5.3278

ρ is bulk resistivity, *η* is chargeability, *MN* is normalized chargeability, and *h* is thickness

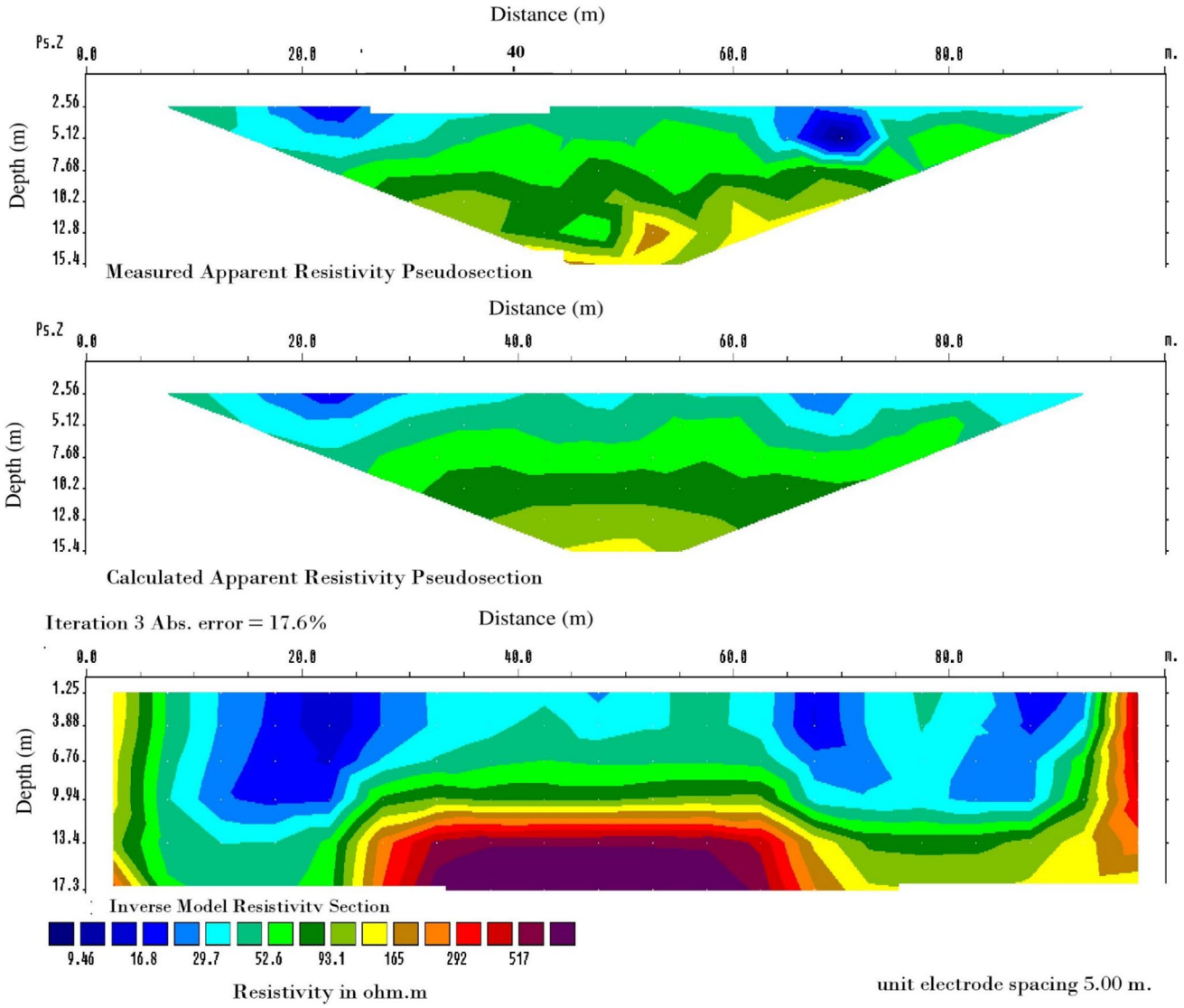

Fig. 9 Inverse model resistivity section at Azikoro Village (low-groundwater Fe site)

Table 4 Chemical composition of the groundwater at high-Fe areas

VES-IP no	Borehole no	Depth (m)	pH	Eh	EC	TDS	Na^+	K^+	Ca^{2+}	Mg^{2+}	Fe	Cl^-	SO_4^{2-}	NO_3^-	HCO_3
VES-IP 6	BH-1	15.2	6.31	118	2250	1125	38.9	14	15	5.7	12.26	18.5	12.4	4.6	40
VES-IP 7	BH-2	30	6.3	125	250	125	7.5	2.4	14.9	3.7	4.5	20	5.5	0.42	2
VES-IP 8	BH-16	21	6.18	128	495	248	13.8	6.5	3.5	1.8	0.86	14.2	4.7	1.6	5.9
VES-IP 9	P-1	20	6.06	116	910	455	12.4	7.6	13.5	3.8	10.1	12.5	2.3	6.74	8.4
VES-IP 10	P-2	15	5.8	133	890	450	10.6	5.8	14.8	12.6	2.08	28.4	1.2	1.68	6.2
VES-IP 11	BH-9	12	6.83	120	212	1060	52.2	24.7	30.4	10.7	0.5	31.8	7.2	0.13	10.8

All parameters have been expressed as mg/L except pH, EC and Eh. The unit of EC is µS/cm, and that of energy potential (Eh) is mV

stratigraphy and lithology across the study area show a near surface aquitard composed of argillaceous materials (clay) widely occurs in the upper most subsurface sediments in the high-Fe locations. This near surface aquitard heterogeneity and variation in thickness lead to variation in vertical recharge, localized dilution and confinement, resulting in varying redox conditions in the aquifer affecting Fe release.

Table 5 Fe concentration in the aquifer sediments

	Borehole no	Redox potential (mV)	Sediment Fe conc. (mg/L)	Groundwater Fe conc. (mg/L)
High-Fe locations	B-1	118	0.75	12.60
	B-2	125	0.26	4.50
	B-16	128	0.30	0.86
	P-1	116	0.9	10.10
	P-9	120	0.79	0.50
Low-Fe locations	B-6	164	0.50	0.16
	B-13	157	0.75	0.14
	B-15	148	0.62	0.26
	B-14	115	0.59	0.20
	P-8	142	0.82	0.22
	P-11	163	n.d	0.02
	P-12	158	n.d	0.18

6 Conclusion

An integrated hydrogeophysical investigation consisting of electrical resistivity and induced polarization techniques in parts of the Niger Delta delineated a widespread clay layer characterized by low resistivity (5–96 Ωm) and high chargeability and normalized chargeability values (0.67–13.9 ms and 0.134–2.242 mS/m) overlying the aquifer in locations that show elevated dissolved Fe concentrations. The thickness of the clay layer varies, pinching out at some places. In locations where the clay layer pinches out, the Fe concentration is within WHO acceptable limits (< 0.3 mg/L), implying that the lithological set-up plays a significant role in understanding Fe enrichment in groundwater in the Niger Delta. The low-permeability clay layer acts a confining layer and thus helps in creating atmosphere-isolated state in the underlying aquifer which is responsible for the reductive ambient subsurface groundwater environment favourable to Fe ions transferring from the aquifer matrix into the groundwater. The knowledge of the clay layer will be very helpful in selecting suitable sites for the installation of boreholes.

Acknowledgements We are grateful to the Post-graduate Geophysics students in the Department of Physics who assisted with the field work and Mr. Udofia for producing the maps.

Compliance with ethical standards

Conflict of interest We do not have conflict of interest in this paper.

References

1. Okiongbo KS, Douglas RK (2013) Hydrogeochemical analysis and evaluation of groundwater quality in Yenagoa city and environs, Southern Nigeria. Ife J Sci 15:209–222
2. Okiongbo KS, Douglas RK (2015) Evaluation of major factors influencing the geochemistry of groundwater using graphical and multivariate statistical methods in Yenagoa City, Southern Nigeria. J Appl Water Sci 5:27–37
3. Ohimain EI, Angaye T, Okiongbo KS (2013) Removal of iron, coliforms and acidity from groundwater obtained from shallow aquifer using trickling Filter method. J Environ Sci Eng A 2:549–555
4. Niwas S, Singhal DC (1981) Estimation of aquifer transmissivity from Dar Zarrouk parameters in porous media. J Hydrol 50:393–399
5. Dhakate R, Singh VS, Negi BC, Chandra S, Rao VA (2008) Geomorphological and geophysical approach for locating favourable groundwater zones in granitic terrain, Andhra Pradesh, India. J Environ Manag 88:1373–1383
6. Okiongbo KS, Mebine P (2015) Estimation of aquifer hydraulic parameters from geoelectric method—A case study of Yenagoa and environs Southern Nigeria. Arab J Geosci 8:6085–6093
7. Akpokodje EU, Etu-Efeotor JO (1987) The occurrence and Economic potential of clean sand deposits of the Niger Delta. J Afr Earth Sci 6:61–65
8. Akpokodje EU (1987) The engineering-geological characteristics and classification of the major superficial soils of the Niger Delta. Eng Geol 23:193–201
9. Akpokodje EG (1986) A method of reducing the cement content of two stabilized Niger Delta soils. Q J Eng. Geol. Lond 19:359–363
10. Amajor LC (1991) Aquifers in the Benin Formation (Miocene—Recent), Eastern Niger Delta, Nigeria. Lithostratigraphy, Hydraulics and water quality. Environ Geol Water Sci 17:85–101
11. Short KC, Stauble AJ (1967) Outline of the geology of the Niger Delta. Bull AAPG 51:761–779

12. Abam TKS (1999) Dynamics and quality of water resources in the Niger Delta. Impacts of urban growth on surface water and groundwater quality. In: Proceedings of IUGG 99 symposium, vol 259. IAHS Publication, Birmigham, pp 429–437
13. Mbonu PDC, Ebeniro JO, Ofoegbu CO, Ekine AS (1991) Geoelectric sounding for the determination ofaquifer characteristics in parts of Umuahia area of Nigeria. Geophysics 56:84–291
14. Ekine AS, Osobonye GT (1996) Surface geoelectric sounding for the determination of aquifer Characteristics in part of Bonny Local Government Area of Rivers State. Niger J Phys 85:93–99
15. Summer JS (1976) Principles of induced polarization for geophysical exploration. Elsevier, Amsterdam
16. Schon JP (1996) Physical properties of rocks: fundamentals and principles of petrophysics. Pergamon, New York, p 583
17. Slater LD, Lesmes D (2002) IP interpretation in environmental investigations. Geophysics 68:77–88
18. Lesmes D, Frye KM (2001) Influence of pore fluid chemistry on the complex conductivity and induced polarization responses of Berea sandstone. J Geophys Res 160:4079–4090
19. Loke MH, Baker RD (1996) Rapid least square inversion of apparent resistivity pseudosections by a quasi-Newton method. Geophys Prospect 44:131–152
20. Griffiths DH, Barker RD (1993) Two-dimensional resistivity imaging and modelling in areas of complex geology. J Appl Geophys 29:211–226
21. Samouelian A, Cousin I, Tabbagh A, Bruand A, Richard G (2005) Electrical resistivity survey in soil science: a review. Soil Tillage Res 83:173–193
22. APHA (1998) Standard methods for the examination of water and wastewater, 19th edn. American Public Health Association, Washington
23. Baines D, Smith DG, Frose DG, Bauman P, Nimack G (2002) Electrical resistivity ground imaging [ERGI]: a new tool for mapping the lithology and geometry of channel-belts and valley-fills. Sedimentology 49:441–449
24. Beresnev IA, Hruby CE, Davis CA (2002) The use of multi-electrode resistivity imaging in gravel prospecting. J Appl Geophys 49:245–254
25. Magnusson MK, Fernlund JMR, Dahlin T (2010) Geoelectrical imaging in the interpretation of geological conditions affecting quarry operations. Bull Eng Geol Environ 69:465–486
26. Amaya AG, Dahlin T, Barmen G, Rosberg JE (2016) Electrical resistivity tomography and induced polarization for mapping the subsurface of alluvial fans: a case study in Punata (Bolivia). Geosciences 6:1–13
27. Vonhala H (1997) Mapping oil contaminated sand and till with spectral induced polarization (IP) method. Geophys Prospect 45:303–326
28. Hasan MA, Ahmed KM, Sracek O, Bhattacharya P, von Brömssen M, Broms S, Fogelström J, Mazumder ML, Jacks G (2007) Arsenic in shallow groundwater of Bangladesh: investigations from three different physiographic settings. Hydrogeol J 15:1507–1522
29. Okiongbo KS, Soronnadi-Ononiwu GC (2016) Characterizing aggregate deposits using electrical resistivity method: case history of sand search in the Niger Delta, Nigeria. J Earth Sci Geotech Eng 8:1–16

Publisher's Note Springer Nature remains neutral with regard to jurisdictional claims in published maps and institutional affiliations.